12202 *Biochemistry* **2009,** *48,* 12202–12212
DOI: 10.1021/bi900624j

BIOCHEMISTRY
including biophysical chemistry & molecular biology
Article

Bruno Protein Contains an Expanded RNA Recognition Motif[†,‡]

Angeline M. Lyon,[§] Brad S. Reveal,[∥,⊥] Paul M. Macdonald,[∥,⊥] and David W. Hoffman*[,§,⊥]

[§]*Department of Chemistry and Biochemistry, and* [∥]*Section of Molecular Cell and Developmental Biology, and* [⊥]*Institute for Cellular and Molecular Biology, University of Texas, Austin, Texas 78712*

Received April 10, 2009; Revised Manuscript Received November 9, 2009

ABSTRACT: The RNA recognition motif (or RRM) is a ubiquitous RNA-binding module present in ~2% of the proteins encoded in the human genome. This work characterizes an expanded RRM, which is present in the *Drosophila* Bruno protein, and targets regulatory elements in the *oskar* mRNA through which Bruno controls translation. In this Bruno RRM, the deletion of 40 amino acids prior to the N-terminus of the canonical RRM resulted in a significantly decreased affinity of the protein for its RNA target. NMR spectroscopy showed that the expanded Bruno RRM contains the familiar RRM fold of four antiparallel β-strands and two α-helices, preceded by a 10-residue loop that contacts helix α_1 and strand β_2; additional amino acids at the N-terminus of the domain are relatively flexible in solution. NMR results also showed that a truncated form of the Bruno RRM, lacking the flexible N-terminal amino acids, forms a stable and complete canonical RRM, so that the loss of RNA binding activity cannot be attributed to disruption of the RRM fold. This expanded Bruno RRM provides a new example of the features that are important for RNA recognition by an RRM-containing protein.

RNA recognition motifs (RRMs)[1] are one of the most common RNA binding domains (*1*). They have been found in plants, prokaryotes, fungi, and animals; in humans, up to 2% of proteins encoded in the genome contain at least one RRM (*1*, *2*). Proteins containing RRMs act in many RNA processing events, including pre-mRNA and mRNA splicing, alternative splicing, RNA editing, mRNA export, pre-mRNA complex formation, mRNA stabilization, localization, translational regulation, and RNA degradation (*3*).

The RRM fold was described by Nagai et al. (*4*) in the crystal structure of the U1A snRNP protein. The canonical RRM structure is composed of four antiparallel β-strands and two α-helices, giving the $\beta_1\alpha_1\beta_2\beta_3\alpha_2\beta_4$ topology of the protein. The α-helices stack on one face of the β-strands. The primary RNA binding site is composed of residues located on strands β_3 and β_1, which contain two highly conserved sequences called ribonucleoprotein 1 (RNP1) and RNP2 (*5*). RNP sequences contain several conserved aromatic amino acids that are exposed to solvent to facilitate RNA binding. Additional contacts with RNA can be made through amino acids at the N- and C-termini of the RRM and internal loops, in particular, the loop between β_2 and β_3 (for reviews, see refs *1*−*3* and *6*−*8*).

Bruno is a *Drosophila* RRM-containing protein that plays a central role in regulation of Oskar (Osk) expression (*10*, *11*). Proper deployment of Oskar at the posterior pole of the oocyte and embryo is crucial for both embryonic body patterning and formation of the germ line. This spatial restriction of Osk expression is achieved through a combination of mRNA localization and translational regulation: translation of unlocalized mRNA is repressed, and only the localized mRNA gives rise to protein (*12*). Bruno mediates repression by binding to regulatory Bruno response elements (BREs) in the *osk* mRNA 3′ UTR (*10*−*13*).

The full-length Bruno protein contains three RRMs, two located in the N-terminal half of the protein and the third near the C-terminus, separated by a linker region (*10*, *11*). Both the sequence and overall domain structure are well conserved in similar proteins found in other species, and in protein families related to Bruno, such as the ELAV, CELF, and Bruno-like protein families (*14*−*22*). During the initial isolation of a Bruno cDNA, a C-terminal portion of Bruno, consisting of the third RRM and the preceding 40 amino acids (now called RRM3+), was found to bind specifically to BREs (*11*), and to do so with high affinity. Interestingly, canonical Bruno RRM3, which lacks the additional N-terminal residues, was found to have significantly reduced binding activity (*13*). In this work, biochemical and biophysical methods were used to address the differences between Bruno RRM3+ and RRM3 in RNA binding.

EXPERIMENTAL PROCEDURES

Protein Coding, Expression, and Purification. Fragments of Bruno RRM3+ were expressed in *Escherichia coli* strain BL21(DE3)pLysS using the pET3a expression plasmid. The RRM3+ construct of amino acids 471−604 was grown in Luria broth to an OD_{590} of 0.4−0.6, followed by induction with 1 mM IPTG. Cells were allowed to grow for an additional 4 h at 37 °C. The cells were harvested and lysed by sonication. Nucleic acids were removed by the addition of 0.5% poly(ethylenimine) (v/v), and the cell lysate was centrifuged for 20 min at 12000 rpm. The soluble fraction was precipitated by addition of ammonium sulfate to 70% saturation and centrifuged for 20 min at

[†]This work was supported in part by Grant F-1353 from the Welch Foundation and Grant GM54409 from the National Institutes of Health.
[‡]Protein Data Bank entry 2KHC; BioMagResBank accession number 16236.
*To whom correspondence should be addressed. E-mail: dhoffman@mail.utexas.edu. Phone: (512) 471-7859. Fax: (512) 471-8696.
[1]Abbreviations: RRM, RNA recognition motif; NOE, nuclear Overhauser effect; NMR, nuclear magnetic resonance; Bru, Bruno; Osk, oskar; UTR, untranslated region; rmsd, root-mean-square deviation; SDS−PAGE, sodium dodecyl sulfate−polyacrylamide gel electrophoresis.

 Published on Web 11/17/2009

12000 rpm. The protein pellet was resuspended in 1 mM potassium phosphate buffer (pH 6.0) and loaded onto a DEAE ion exchange column. The protein was collected in the flow-through and column wash. The flow-through and wash were combined and diluted to a total volume of 1000 mL with 1 mM potassium phosphate buffer (pH 6.0). The protein was loaded onto a CM Sepharose column and eluted with a 0 to 1 M NaCl gradient. Fractions containing Bruno RRM3+ were identified using SDS−PAGE, pooled, and concentrated. The typical yield of purified Bruno RRM3+ was 4 mg/L of cell culture. Protein samples were dialyzed two times against 1500 mL of 1 mM potassium phosphate buffer (pH 6) and 100 mM sodium chloride; the sample pH was confirmed using a pH meter. N-Terminal sequencing and mass spectrometry were used to confirm the identity of the protein. Samples of Bruno RRM3+ enriched in ^{15}N and/or ^{13}C were prepared as described above, but using M9 minimal medium containing 0.7 g/L [^{15}N]ammonium chloride and/or 2 g of [^{13}C]glucose (Cambridge Isotope Laboratories) as the source of nitrogen and/or carbon. Truncated Bruno RRM3 consisting of amino acids 511−604 was expressed and purified following the same protocol for full-length Bruno RRM3+.

RNA Preparation and Binding Assays. The *osk* 3′ UTR AB RNA (*10*) was labeled with [α-^{32}P]UTP (Perkin-Elmer, BLU507H) by in vitro transcription with Sp6 RNA polymerase (NEB, 207S). Gel-purified RNA at a concentration of 200 pM was incubated with purified RRM3 or RRM3+ for 60 min at room temperature in 50 μL of 1× binding buffer [20 mM HEPES (pH 7.9), 100 mM KCl, and 2 mM $MgCl_2$]; protein concentrations were in the 0−750 nM range. The reaction mixture was passed sequentially through nitrocellulose (Whatman, catalog no. 10-401-196) (to capture RNA−protein complexes) and nylon (Amersham Biosciences, RPN119B) (to capture unbound RNA) filters using a dot blot apparatus (Whatman, catalog no. 10-447-900), modified as described in ref *23*. Prior to binding, the filters were incubated separately in binding buffer for 30 min and then prewashed with 50 μL of binding buffer in the dot blot apparatus. After binding, the filters were washed with 350 μL of binding buffer, and RNA levels were determined by phosphorimaging (Molecular Imager PharosFX System, Bio-Rad, catalog no. 170-9450). Binding reactions were conducted in triplicate for two independent preparations of the proteins and RNA. Bound RNA/total RNA plot points were fit to a simple hyperbolic equation and the Hill equation; the Hill equation was found to provide a significantly better fit in evaluating RNA binding by the RRM3+ and RRM3 proteins.

NMR Spectroscopy. NMR spectra were recorded at 25 °C using a 500 MHz Varian Inova spectrometer equipped with a triple-resonance probe and *z*-axis pulsed field gradient. NMR samples contained 0.9−3.0 mM Bruno RRM3+ protein in a 90% H_2O/10% D_2O mixture or 99.9% D_2O with 1 mM sodium azide and 1 mM potassium phosphate (pH 6.0). Backbone resonance assignments were obtained from three-dimensional HNCA, HNCACB, and HN(CO)CACB spectra (*24*), HNCO spectra (*25*), and HACACBCO spectra (*26*), which correlate the backbone protons to the N, C^{α}, C, and C^{β} signals within the same amino acid and adjacent amino acids. Side chain resonance assignments were obtained by analyzing three-dimensional (3D) ^{15}N-resolved TOCSY-HSQC and ^{13}C-resolved HCCH-TOCSY and two-dimensional (2D) homonuclear 2QF-COSY and TOCSY spectra (*27*). NOE cross-peaks were detected using 2D $^{1}H-^{1}H$ NOESY, 3D $^{1}H-^{1}H-^{15}N$ NOESY-HSQC, and 3D $^{1}H-^{1}H-^{13}C$ NOESY-HSQC spectra (*28*); spectra with mixing times of 60−150 ms were recorded, with the 60 ms mixing time being used to minimize the effects of spin diffusion. NMR data were processed using NMR-Pipe (*29*). ^{1}H, ^{15}N, and ^{13}C were referenced with proton chemical shifts relative to internal 2,2-dimethyl-2-silapentane-5-sulfonate (DSS) at 0 ppm (*30*). The 0 ppm ^{15}N and ^{13}C reference frequencies were determined by multiplying the 0 ppm ^{1}H reference frequency by 0.101329118 and 0.251449530, respectively.

$^{15}N-^{1}H$ heteronuclear NOE and ^{15}N T_1 and T_2 relaxation times were measured using pulse sequences that feature gradient selection, sensitivity enhancement, and pulses for minimizing saturation of solvent water (*31*). The $^{15}N-^{1}H$ heteronuclear NOE was measured through a comparison of spectra acquired with either a 5 s delay between each free induction decay or a 2 s delay followed by a 3 s series of 120° nonselective ^{1}H pulses. For T_1 relaxation measurements, 2D spectra with relaxation delays of 10, 260, 510, 760, and 1010 ms were recorded. For T_2 relaxation measurements, 2D spectra with relaxation delays of 29, 58, 87, 116, and 145 ms were acquired. For both T_1 and T_2 measurements, the relaxation delay between each acquisition of the free induction decay was 3 s. These relaxation times were calculated from fitting peak heights to a first-order exponential decay equation. Uncertainties in T_1 and T_2 were estimated from the standard deviations in the fit. Rotational correlation times for Bruno RRM3+ and Bruno RRM3 were calculated using Modelfree 4.20 (*32*−*34*) as previously described (*35*). Order parameters for Bruno RRM3+ and Bruno RRM3 were determined using $^{15}N-^{1}H$ NOE, T_1, and T_2 relaxation data and Modelfree version 4.2 (*32*−*34*).

Amide Proton Exchange Rates. For amide protons that exchange relatively slowly with deuterated solvent (with half-times for exchange greater than approximately 5 min), exchange rates were determined as follows. The Bruno RRM3+ and Bruno RRM3 samples were frozen, lyophilized, and resuspended in D_2O. A series of six $^{15}N-^{1}H$ HSQC spectra were acquired and processed identically, and exchange rates were determined by fitting peak heights to a first-order exponential decay equation. Uncertainty in exchange rates was determined from the standard deviation of each fit. For protons that exchange relatively rapidly with solvent (on the order of seconds), saturation transfer experiments were conducted for Bruno RRM3+ and Bruno RRM3 at pH 6 and 8, and the data were fit as described by Lillemoen et al. (*36*). For the saturation transfer experiments, T_1 values for amide protons in uniformly ^{15}N-labeled Bruno RRM3+ and Bruno RRM3 were estimated using an inversion recovery experiment, and found to be 721 and 822 ms, respectively. For amide protons with exchange rates that fell between the ranges accessible by the deuterium transfer or saturation transfer methods, rates were assigned in this intermediate range, with appropriate uncertainties. The amide exchange rates (Tables S1 and S2 of the Supporting Information) were normalized to pH 7 by assuming a 1 unit pH change corresponds to a 10-fold change in the exchange rate, as assumed in the EX2 exchange regime (*37*−*40*). Amide proton protection factors were calculated according to the method previously described by Bai et al. (*37*); these calculated protection factors include corrections for the influence of primary sequence on amide proton exchange rate (*37*).

Structure Calculation. Structure calculations for Bruno RRM3+ were performed using a restrained simulated annealing protocol within CNS version 1.1 (*41*). Calculations were

conducted with the goal of determining the full range of structures that satisfy distance and angle restraints derived from the NMR data, while maintaining reasonable molecular geometry, consistent with a minimum value for the CNS energy function. Distance constraints were derived from the intensities of cross-peaks within homonuclear 2D NOE spectra with mixing times of 60−200 msec and 3D ^{15}N- and ^{13}C-resolved NOE spectra acquired with mixing times of 120−150 ms. On the basis of the cross-peak intensities in the NOE spectra, the distance restraints were sorted into four categories: strong (< 3.50 Å), medium (< 4.20 Å), weak (< 5.00 Å), and very weak (< 6.00 Å). Pseudoatom corrections were also applied to the distance constraints described above: NOEs from valine or leucine methyl groups that were not stereospecifically assigned were measured from the center of the two methyl groups, adding 2.4 Å to the interproton distance. For NOEs involving other methyl protons, distances were measured from the center of the methyl group, and 1.0 Å was added to the interproton distance. For NOEs involving methylene protons that were not stereospecifically assigned, distances were measured from the center of the methylene group, and 0.7 Å was added to the interproton distance. For NOEs involving the δ- and ε-protons on tyrosine and phenylalanine rings, the distance was measured from the center of the two δ- or ε-protons, and 2.4 Å was added to the interproton distance restraint. The PREDITOR torsion angle prediction program was used to assign ϕ and ψ angle restraints for backbone atoms based on the chemical shifts of C^{α}, N, HN, H^{α}, C^{β}, and C (*42*). Hydrogen bonds were defined using distance bounds for amide protons that were clearly located within the regions of regular β-sheet and α-helical structure.

Twenty-five diverse starting structures for RRM3+ were generated by subjecting a random coil model to the CNS simulated annealing protocol using only dihedral angle constraints. These 25 structures were used as starting models for 100 runs of the simulated annealing protocol for each model. Most simulated annealing runs generated similar structures with similar energies. From this final set of refined models, a set of 18 structures were selected on the basis of (i) their CNS energy being at or very close to the minimum value obtained, (ii) the fact that there were no interproton distance constraint violations greater than 0.6 Å, and (iii) the fact that the set of models are a fair representation of the total range of structures generated that satisfy the NMR-derived distance restraints while maintaining reasonable molecular geometry, as defined by the CNS energy function. Chemical shifts for Bruno RRM3+ have been submitted to the BioMagResBank and assigned accession number 16236. Coordinates for Bruno RRM3+ have been submitted to the Protein Data Bank (PDB) as entry 2KHC.

Circular Dichroism Spectroscopy. Circular dichroism spectra were recorded using a JASCO J-815 instrument. All data were collected in 1 nm intervals between 185 and 260 nm. Each scan was collected three times, and the signals were averaged. Temperature dependence spectra were recorded between 5 and 45 °C at 5 °C intervals. The samples were allowed to equilibrate at each temperature for 10 min prior to data collection. Before data collection, samples were dialyzed against 1 mM potassium phosphate and 100 mM Na_2SO_4 (pH 6); the sample pH was confirmed by measurement with a pH meter. Sodium sulfate was used in place of the sodium chloride used in NMR samples, as it is more transparent in the far-UV range. Protein concentrations were calculated using extinction coefficients of 3.47×10^5 and 4.55×10^5 M^{-1} cm^{-1} at 205 nm for Bruno RRM3 and RRM3+, respectively. The CD data were converted to mean residue ellipticity, and secondary structure was determined using SOMCD (*50*).

RESULTS

The Bruno protein binds Bruno response elements (BREs) located within the 3′ UTR of *oskar* mRNA. Previous work identified a 127-nucleotide RNA sequence from *oskar* (termed the *osk* AB RNA) that is sufficient for Bruno binding and translational repression (*10*, *11*, *13*) (Figure S1 of the Supporting Information). This *osk* AB RNA was previously used to identify a minimal RNA binding domain for the RRM closest to the C-terminus of Bruno in UV cross-linking experiments (*13*). In this work, in vitro filter binding assays were used to measure the affinity for the *osk* AB RNA for two versions of the C-terminal RRM domain, termed RRM3 and RRM3+. RRM3+ (containing residues 471−604 of Bruno) includes the canonical RRM with additional N-terminal residues previously shown to significantly enhance RNA binding (*13*); RRM3 contains the complete canonical RRM but lacks the residues prior to residue 510. Data obtained from the filter binding assays were fit to a simple hyperbolic equation and a sigmoidal Hill equation. The Hill equation was found to provide a significantly better fit, with $K_{1/2}$ values for RRM3+ and RRM3 of 124 and 566 nM, respectively (Figure 1). Fitting to the Hill equation raises the possibility of multiple binding sites and cooperative behavior. This is plausible, since the relatively large size of the 140-nucleotide RNA (compared to the protein domain) could permit multiple copies of the recognition sequence to be present. However, the basis of any potential cooperative binding behavior remains speculative at this time, given that the RNA recognition sequence and details of protein−RNA interactions are not yet precisely defined.

NMR studies were undertaken to improve our understanding of the structure and dynamics of Bruno RRM3 and RRM3+ and gain insight regarding their differing abilities to bind RNA.

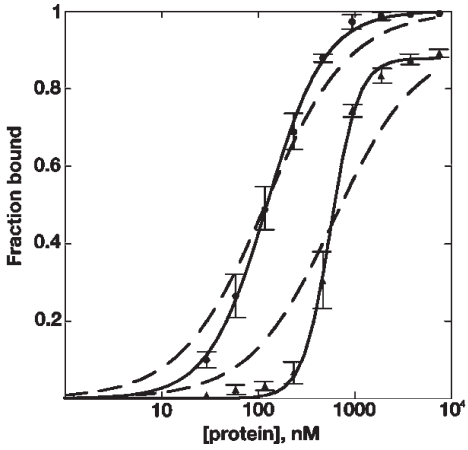

FIGURE 1: Bruno RRM3+−*osk* mRNA interactions. Comparison of the binding of Bruno RRM3 and Bruno RRM3+ to the *oskar* AB region RNA, derived from filter binding data. Binding of RRM3+ is indicated by filled circles, while binding of RRM3 is indicated by filled triangles. The binding data for the two proteins were fit to the Hill equation: $y = (y_{max}[E]^c)/(K_{1/2}{}^c + [E]^c)$. $K_{1/2}$ for the RRM3+ protein is 124 nM with a coefficient of cooperativity of 1.4; $K_{1/2}$ for the RRM3 protein is 566 nM with a coefficient of cooperativity of 3.1. For comparison, fits to a hyberbolic binding equation are shown using dashed lines. The RNA concentration was 200 pM; protein concentrations were in the 0−750 nM range.

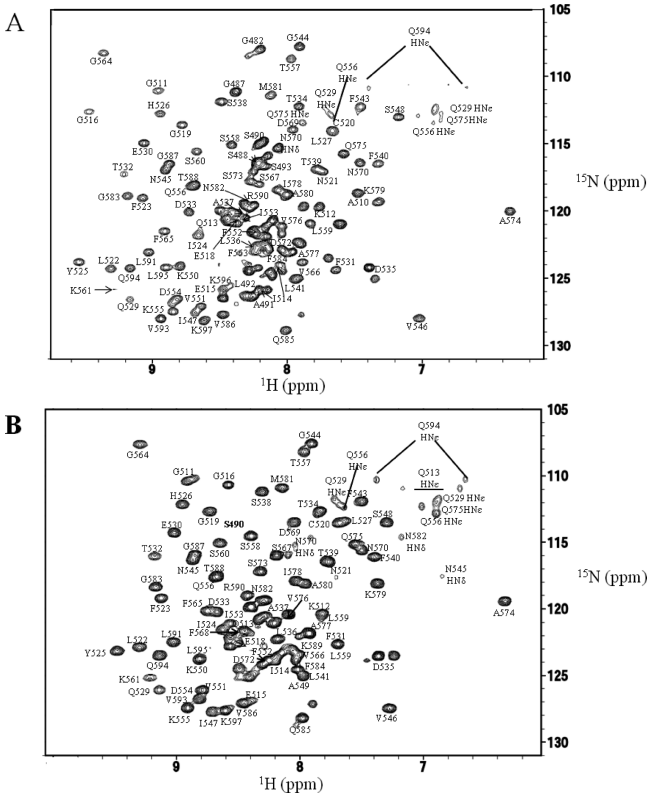

FIGURE 2: ^{15}N−^{1}H HSQC spectra of Bruno RRM3+ and Bruno RRM3. Spectra were recorded at pH 6 and 25 °C. (A) Representative spectrum for Bruno RRM3+. (B) Representative spectrum for Bruno RRM. Peaks that are well-resolved in the 2D spectra are labeled. Residues 512, 531, and 535 have doubled peaks, which may be due to the presence of multiple conformations of these residues.

Bruno RRM3 and RRM3+ were each found to be suitable for NMR studies (Figure 2 and Figure S2 of the Supporting Information). The freshly prepared protein appeared as a single band by SDS−PAGE; however, N-terminal sequencing and mass spectrometry indicated that Bruno RRM3+ was heterogeneous in the several amino acids nearest the N- and C-termini, presumably due to proteolytic cleavage or degradation. Three-dimensional and triple-resonance NMR methods were used to obtain spectrum assignments and structural information for residues 480−597 of RRM3+, where residues are numbered consistent with the full-length Bruno protein (Figure 2). The integrity of the protein samples was monitored using NMR spectra and SDS−PAGE. Structural statistics for Bruno RRM3+ are summarized in Table 1.

The dominant structural feature of RRM3+ is a sheet comprised of four antiparallel β-strands, formed by residues 520−597; this is termed the canonical RRM. The two α-helices cross one face of the antiparallel β-sheet (Figure 3). The connections between β_1 and β_2 and between β_3 and β_4 are formed through the two α-helices, with α_1 connecting β_1 to β_2 and α_2 connecting β_3 to β_4. The four-strand antiparallel β-sheet and helices α_1 and α_2 that form the canonical RRM are all well-defined by the NMR-derived distance restraints (Figure 3). The ribonucleoprotein-1 (RNP1) and RNP2 sequences that are well-conserved among RRM-containing proteins (Figure 4) are located within β_3 and β_1, respectively; these β-strands are the central strands in the structure. In Bruno RRM3+, the RNP2 motif contains residues N521, F523, and Y525, and the RNP1 motif contains F563, F565, S567, and D569, with these side chains exposed on the protein surface which is typical in RRM

Table 1: Summary of Refinement and Structural Statistics Obtained for the *Drosophila melanogaster* Bruno RRM3+ Protein[a]

no. of intraresidue NOEs	479
no. of sequential NOEs (from residue i to $i+1$)	433
no. of medium-range NOEs (from residue i to $i+2$, $i+3$, $i+4$)	284
no. of long-range NOEs	428
no. of dihederal angle restraints (ϕ and ψ)	224
no. of hydrogen bond restraints	36
total no. of structural restraints	1884
rmsd for backbone atoms (residues 510−597) (Å)	0.59
rmsd for all atoms (residues 510−597) (Å)	1.31
rmsd for backbone atoms (residues 520−597, excluding loops) (Å)	0.45
rmsd for all atoms (residues 520−597, excluding loops) (Å)	1.00
average no. of NOE violations >0.2 Å (per structure)	7.4
average no. of NOE violations >0.6 Å (per structure)	0
residues in the most favored regions of the Ramachandran plot	78.3%
residues in the additional allowed regions of the Ramachandran plot	19.9%
residues in generously allowed regions of the Ramachandran plot	1.8%
rmsd for covalent bonds (for all atoms) (Å)	0.0057
rmsd for covalent angles (for all atoms) (deg)	0.91

[a]Statistics are derived from a set of 18 low-energy structures, each obtained by simulated annealing, with no more than two models derived from each unique starting model.

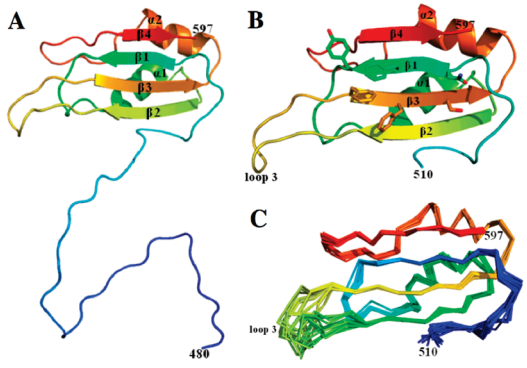

FIGURE 3: (A) Ribbon diagram of amino acids 480−597 of Bruno RRM3+, showing the canonical RRM (residues 520−597) as well as the additional N-terminal amino acids. It should be emphasized that structures of the N-terminal residues (480−509) are not well-defined, and the NMR data support their being flexible in solution. The protein is color-ramped from blue at the N-terminus to red at the C-terminus. (B) Ribbon diagram showing residues 510−597 of Bruno RRM3+, with side chains shown for residues F563, F566, and S567 in the conserved RNP1 sequence in β_3 and N521, F523, and Y525 in the conserved RNP2 in β_1; these solvent-exposed residues are likely to be involved in RNA binding. (C) Eighteen low-energy structures of Bruno RRM3+ that fit the NMR-derived constraints equally well are superimposed, with residues 510−597 displayed. The superposition was obtained by minimizing the differences in the coordinates of the backbone atoms for residues 510−597. These 18 structures are a fair representation of the full range that is consistent with the NMR-derived constraints while maintaining reasonable molecular geometry. The diagrams were created using PyMol (*59*).

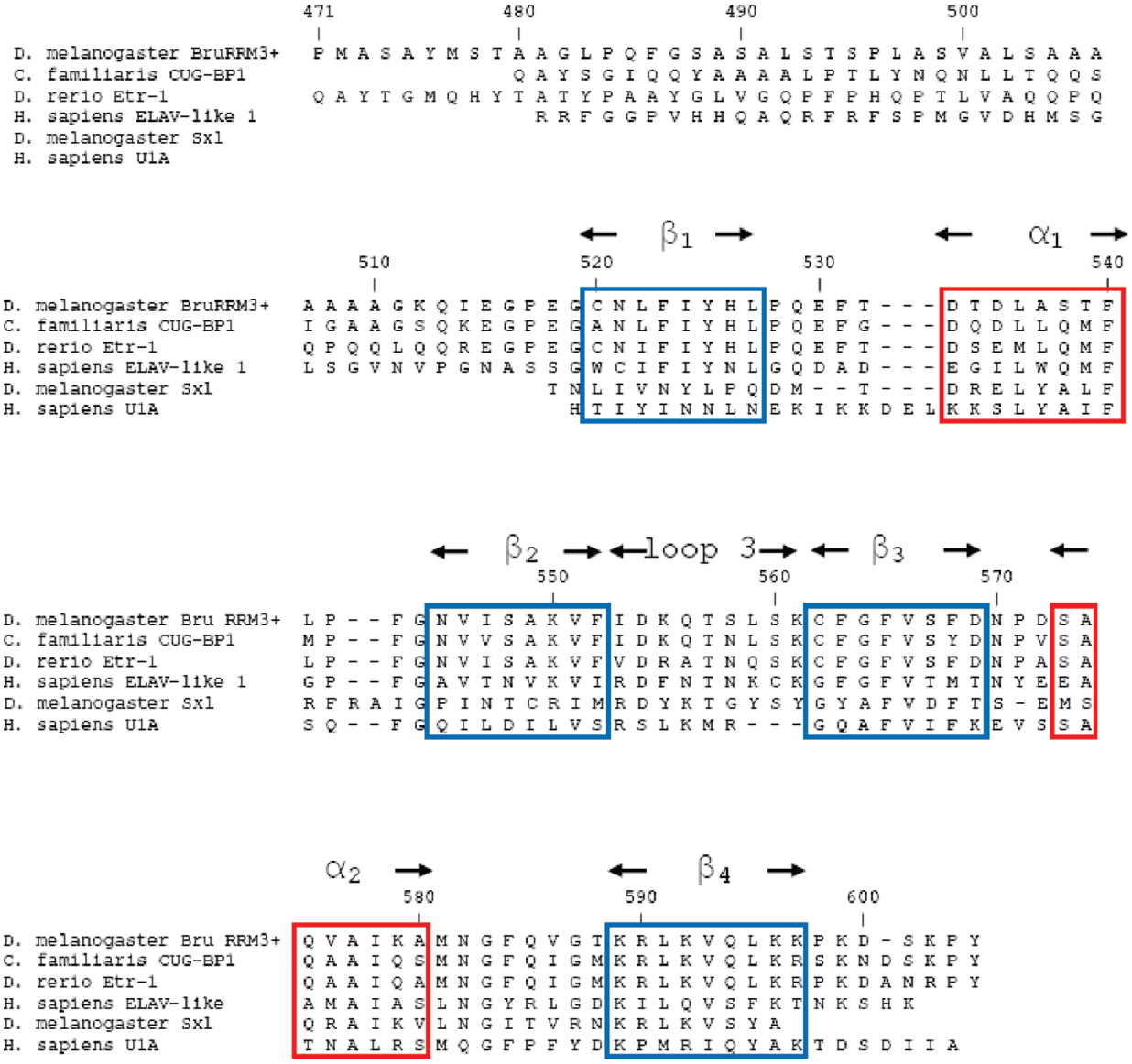

FIGURE 4: Sequence alignment of Bruno RRM3+. Amino acids of RRM3+ of the *D. melanogaster* Bruno protein are aligned with similar sequences from other eukaryotic species. Aligned sequences include *Canis familiaris* CUG-binding protein-1, *Danio rerio* ELAV-type ribonucleoprotein-1, *H. sapiens* embryonic lethal abnormal visual-like protein, *D. melanogaster* sex-lethal protein, and *H. sapiens* U1A protein. Conserved β-strands are boxed in blue, and conserved regions of α-helix are boxed in red. The ribonucleoprotein-1 (RNP1) and RNP2 sequences common to the RRM-containing proteins are located within β_3 and β_1, respectively.

structures. The core of Bruno RRM3+ is formed by conserved hydrophobic residues, with side chains pointing toward the interior of the protein. Within the sheet structure, β_2 and β_3 are connected by an extended loop (labeled loop 3 in Figure 3); this loop has been shown to be involved in RNA recognition and binding in other RRM structures, in particular, the U1A N-terminal RRM (*43*−*47*). Interestingly, Bruno RRM3+ contains a cysteine residue (C562) at the link between loop 3 and β_2, in the same position as a well-conserved glycine in human U1A RRM1. Previous work has shown that this particular glycine residue is important in correlating motions in the loop with the conserved aromatic residues in RNP1 and RNP2 (*46*, *47*). Given this change, it is possible that the cysteine in this position in Bruno may alter any potential interactions between loop 3 and the residues of the central two β-strands. In Bruno RRM3+, loop 3 is on the same face of the RNA binding surface as RNP1 and RNP2 and is located adjacent to solvent-exposed hydrophobic residues in RNP1. The canonical RRM within Bruno RRM3+ is similar to the well-characterized RRMs from U1A protein (residues 10−87 of PDB entry 1OIA) (*4*) and the *D. melanogaster* sex-lethal protein (residues 125−200 of PDB entry 1B7F) (*48*), with rmsd values of 1.92 and 2.16 Å, respectively, when the backbones of the strands and helices are superimposed.

NMR data showed that residues G511 and K512, which are located prior to the canonical RRM, have multiple long-range $^1H-^1H$ NOEs indicating that they contact D533 and T534 of helix α_1 as well as residues 546−549 and 551 within strand β_2. Similar interactions have been previously described for only one other RRM, RRM3 of the CUG-binding protein (PDB entry 2CPZ) (*49*). Residues 512, 531, 535, and 559 were observed to have doubled peaks in the NMR spectra of Bruno RRM3+ (Figure 2), which may be a result of multiple conformations of these residues.

In the case of RRM3+, the NMR data provided no long-range distance restraints for residues 480−510 and 513−516; therefore, the positions of these N-terminal residues are not well-defined in

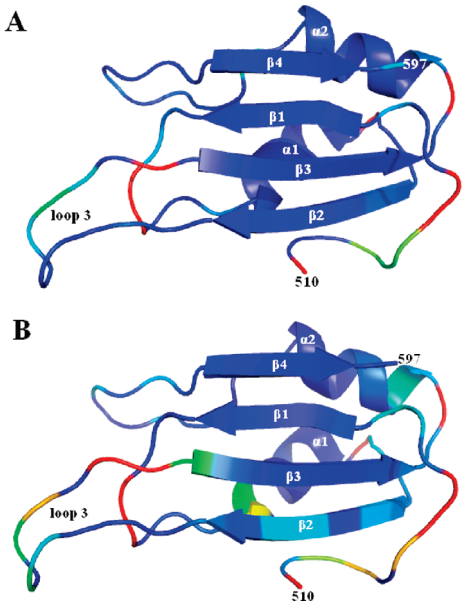

FIGURE 5: Order parameters for RRM3+ and RRM3. The diagram summarizes the order parameters (S^2) for residues 510−597, calculated from ^{15}N relaxation data for the backbone amide groups. The figures are color-ramped from blue to red, with blue indicating residues with the highest order parameters (>0.95) and, therefore, in relatively well-ordered structure. Red indicates residues with order parameters as low as 0.3 and, therefore, relatively flexible structure. For residues for which order parameters were not determined, such as prolines, those with rapidly exchanging amide protons, and those not resolved in 2D spectra, colors were assigned on the basis of adjacent residues. The full set of order parameters appears in Figures S3 and S4 of the Supporting Information. (A) Order parameters for residues 510−597 of RRM3+. The flexible residues prior to residue 510 are not shown. (B) Order parameters for truncated Bruno RRM3, which lacks the flexible N-terminal residues prior to residue 510. These figures were created using PyMol (*59*).

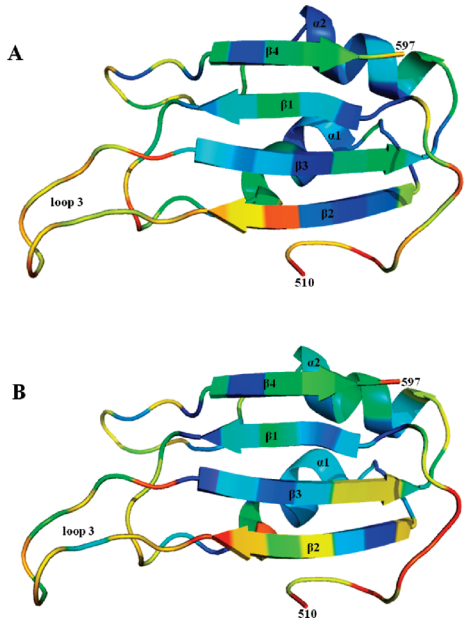

FIGURE 6: Amide proton protection factors. The diagram summarizes the backbone amide proton protection factors (*P*) for Bruno RRM3+ and Bruno RRM3 at 25 °C. Residues are color-ramped from red to blue, with red indicating residues with small log *P* values; the full range of log *P* values is −2.2 to 5.6. For residues for which no amide protection factor was determined, such as prolines and those not resolved due to spectral overlap, residues are colored on the basis of adjacent amino acids. The full set of amide protection factors appears in Tables S3 and S4 of the Supporting Information. (A) Protection factors for residues 510−597 of Bruno RRM3+. Residues 480−509 are not shown, but would be colored red as their amide protons are not well protected from solvent exchange. (B) Protection factors for Bruno RRM3, which lacks the amino acids prior to residue 510. These figures were created using PyMol (*59*).

the structural models. The majority of the residues have backbone chemical shifts that are consistent with extended structure, and the lack of observable NOE peaks is consistent with these residues being flexible or in equilibrium between multiple conformations.

NMR spectroscopy provides several tools that can be used to probe the dynamics of a protein in solution. ^{15}N relaxation rates and ^{15}N−^{1}H heteronuclear NOEs were measured for the backbone amide groups of Bruno RRM3+, to establish the relative flexibility of various regions of the protein structure in solution. The ^{15}N relaxation and ^{15}N−^{1}H NOE data were analyzed using Modelfree4 (*32*) for the purpose of assigning order parameters (*33*, *34*) to the individual backbone amide groups. Data for Bruno RRM3+ were fit using a model of simple isotropic diffusion, where the tumbling of the molecule was described by a single overall rotational correlation time (τ_m) of 8.0 ns. Individual order parameters (between 0 and 1) were used to describe how closely the motion of each backbone amide group was coupled to the overall tumbling time of the molecule (Figure 5 and Figures S3 and S4 of the Supporting Information). Relatively large order parameters and positive ^{15}N−^{1}H heteronuclear NOEs are indicative of well-ordered structure, while smaller order parameters and negative or near-zero ^{15}N−^{1}H NOEs indicate flexibility. Beginning at the N-terminus of the protein, the first residues to exhibit order parameters of >0.6 and positive ^{15}N−^{1}H NOEs are residues 511 and 512, which contact β_2 and α_1 of the RRM domain. Residues prior to residue 511 with detectable NMR signals that were not obscured by overlap exhibited order parameters of <0.6 and negative or near-zero ^{15}N−^{1}H NOEs, consistent with them being relatively flexible in solution. Relaxation rate data were not obtained for residues 480, 490, 491, and 494−509 within the N-terminal extension, due to resonance overlap in the 2D spectra or lack of observable ^{15}N−^{1}H signals, likely due to rapid exchange with the solvent. Other residues with relatively low order parameters are residues 513−515, which connect ordered residues 511 and 512 with the canonical RRM, and residues 559 and 560 in loop 3, just prior to the start of β_3, and residue 582, which is the second residue in the loop connecting α_2 to β_4. Nearly all other residues within the canonical RRM (residues 520−597) have order parameters of ≥0.8, consistent with a relatively ordered structure (Figure 5 and Tables S3 and S4 of the Supporting Information). Order parameters were only slightly changed if anisotropic (rather than isotropic) diffusion was assumed, with axial ratios in the 0.8−1.3 range; these small differences in order parameters that depend on the choice of diffusion model are reflected in the uncertainties of the order parameters.

The rates at which backbone amide protons exchange with solvent provide another source of information regarding protein dynamics. Backbone amide protons may be protected from exchange with solvent if they are involved in relatively stable hydrogen bonds or buried within the protein structure. In the case of Bruno RRM3+, 28 amino acids were identified as having relatively slow amide exchange rates (Figure 6 and Tables S1 and S2 of the Supporting Information). These residues were all located within the four regular β-strands or two regular helices of the canonical RRM. The amide protons of the N-terminal

residues of Bruno RRM3+ (those prior to residue 520) exhibit relatively rapid exchange rates (Table S1 of the Supporting Information), consistent with a lack of persistent hydrogen bonds, greater flexibility, and/or solvent accessibility in an EX2 regime (*37*−*40*). Interestingly, residue 549, located within β_2, has a relatively low protection factor compared to the adjacent amino acids. Residue 549 interacts with residues 511 and 512 within the N-terminal region of the RRM3+ protein; the reduced level of protection observed for this residue may be the result of the interaction with these N-terminal residues.

There are two potential explanations for the observation that the relatively flexible N-terminal amino acids of Bruno RRM3+ are required for high-affinity binding of RNA. First, these N-terminal residues may be directly involved in contacting the RNA target. A second possibility is that the N-terminal residues do not directly bind the RNA; however, their removal destabilizes or disrupts the canonical RRM structure, which actually provides the essential RNA contacts. To distinguish between these two possibilities, NMR was used to investigate a construct that contains the full canonical RRM portion of Bruno RRM3+ but omits the flexible N-terminal amino acids and has significantly weakened RNA binding ability (Figure 1); this truncated protein consisted of residues 510−604 (and is termed RRM3). NMR spectra showed this smaller construct formed the four-strand antiparallel β-sheet and two α-helices typical of a complete canonical RRM. This smaller domain was stable in solution and contained amide protons that were protected from exchange with solvent for hours (Table S2 of the Supporting Information), indicating that the flexible N-terminal residues are not required for maintaining the fold of the canonical RRM fold within RRM3+. The results, therefore, support a model in which the N-terminal residues of the Bruno RRM3+ protein are directly involved in RNA binding, and the canonical RRM by itself does not contain all of the essential elements for high-affinity binding of the target RNA.

Comparative NMR studies were used to investigate whether the omission of the flexible N-terminal residues required for RNA binding perturbs the structure and/or dynamics of canonical Bruno RRM3. Specifically, NMR chemical shift assignment, ^{15}N relaxation, ^{15}N−^{1}H NOE, and amide exchange rate data were obtained for Bruno RRM3 (lacking the flexible N-terminal residues prior to residue 510) and then compared with the corresponding data for the longer RRM3+ (Figures 5−7 and Tables S3 and S4 of the Supporting Information). It was found that omitting the flexible N-terminus resulted in some significant chemical shift changes within the canonical RRM, with the

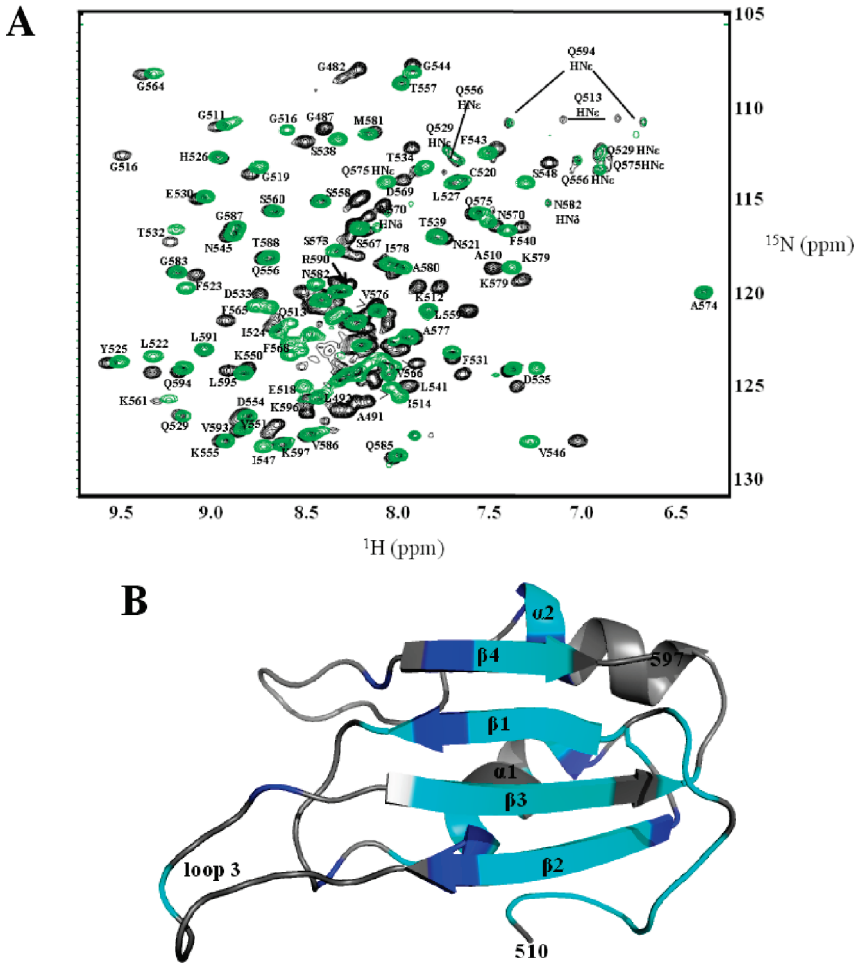

FIGURE 7: Chemical shift perturbations. (A) Overlay of ^{15}N−^{1}H HSQC spectra of Bruno RRM3+ (black) and Bruno RRM3 (green) illustrating the chemical shift differences in amide nitrogens and protons, with clearly resolved peaks labeled. Residues 512, 531, and 535 have doubled peaks, which may be due to the presence of multiple conformations of these residues. (B) Color-coded map showing the regions that exhibit the greatest backbone chemical shift differences between Bruno RRM3+ and Bruno RRM3. Residues with amide proton or nitrogen chemical shift differences of >0.1 and >0.4 ppm, respectively, are colored cyan; residues with chemical shift differences between 0.05 and 0.1 ppm (proton) and 0.2 and 0.4 ppm (nitrogen) are colored blue, and residues with smaller chemical shift changes are colored gray. Three-dimensional NMR spectra were used in evaluating chemical shift perturbations in the relatively crowded regions of the spectra.

largest changes (exceeding 0.1 ppm for ^{1}H) occurring in residues located primarily in or near strands β_1 and β_3 (Figure 7). Interestingly, these two strands contain the RNP1 and RNP2 motifs that contain the primary RNA-binding residues in other RRM-containing proteins (*5*). These chemical shift differences may be attributed to transient interactions between the flexible N-terminal residues and the face of the β-sheet that alter the average magnetic environment without forming any stable structure. Amide proton exchange rates were also determined for Bruno RRM3 and compared to those of RRM3+. Bruno RRM3 was found to have 25 amino acids with high amide protection factors. However, in contrast to the Bruno RRM3+ protein, amide protons in Bruno RRM3 generally exchange more rapidly in this smaller protein (Figure 6). This is consistent with greater hydrogen bond opening frequencies in the truncated domain. Additionally, omitting the N-terminal residues resulted in altered ^{15}N relaxation rates (and reduced order parameters) for a number of residues within RRM3, with the most significant differences occurring in the 10-residue loop 3 that connects strands β_2 and β_3 (Figure 5 and Figures S3 and S4 of the Supporting Information). For several of these loop 3 residues within the truncated RRM3 protein, it was necessary to introduce a chemical exchange term to model their ^{15}N relaxation behavior, indicating more complexity in their motions. The relaxation data for RRM3 are consistent with an overall rotational correlation time (τ_m) of 8.0 ns, not significantly different from that of the Bruno RRM3+ protein. The circular dichroism spectra of the RRM3 and RRM3+ proteins are similar and do not exhibit a substantial temperature dependence in the range of 5−45 °C (Figure 8); these observations are consistent with the conclusion that the amino acids in RRM3+ prior to residue 510 do not contain regular and stable secondary structure.

In summary, the NMR results indicate that omitting the flexible N-terminal residues does not prevent the folding of RRM3 but does result in changes in the chemical shifts, ^{15}N relaxation, and amide exchange rates of some residues, with most of the significant changes occurring in the regions of β_1, β_3, and loop 3. A possible explanation for these observations is that the flexible N-terminal extension, though not well-ordered itself, transiently interacts with the β_1, β_3, and loop 3 regions of the RRM, altering their average environment

DISCUSSION

Although Bruno RRM3+ is unusual in having an N-terminal extension that significantly enhances RNA binding, there are precedents for additional structural elements that expand on the standard RRM fold. For example, in the structure of the polypyrimidine tract binding protein (PTB), the two central RRMs, RRM2 and RRM3, have an additional β-strand at the C-terminus of each motif (*51*, *52*). For PTB RRM3, the absence of the β_5 strand does not impair RNA binding in comparison to that of full-length RRM3. The β_5 strand is also seen in PTB proteins from other species, but whether it represents an expansion on the canonical RRM for additional proteins is unknown (*51*, *52*). The N-terminal RRM of the U1A protein was also found to have an additional α-helix at its C-terminus. This helix became more ordered upon binding RNA and was proposed to act as an additional regulatory element in RNA binding (*4*, *53*, *54*). Truncations of this C-terminal helical extension were shown to impact binding affinity and, to a greater extent, the sequence specificity the protein had for its RNA targets (*53*, *54*). A structure of RRM3 from a Bruno-related protein, CUG-BP, is very similar to that of Bruno RRM3+. CUG-BP RRM3 (PDB entry 2CPZ) has two residues equivalent to G511 and K512 of Bruno RRM3+ that contact residues in strand β_2 and helix α_1 (*49*).

While the N-terminal residues of Bruno RRM3+ are flexible in solution, it is possible that these residues become ordered upon RNA binding. Given that these amino acids have been demonstrated to be required for increased specificity and affinity for RNA binding (*13*) (Figure 1), a conformational change could facilitate additional RNA−protein interactions outside the canonical RRM. Changes in flexible regions upon RNA binding have been previously reported in a several other RRM-containing proteins. In the case of the sex-lethal protein, there are two RRMs connected by a flexible linker region. Upon RNA binding, the linker region becomes ordered and orients the two RRMs such that the RNA is bound in a cleft created by the β-sheets of the two RRMs (*48*). A similar conformational change has been reported in polypyrimidine tract binding protein (PTB). The linker region between PTB RRM3 and RRM4 has been demonstrated through NMR methods to undergo a disordered to ordered transition upon RNA binding, forming a compact globular structure (*7*). In the case of Bruno RRM3+, the interactions of N-terminal residues with α_1 and β_2 raise the possibility that N-terminal residues 480−510 could make contacts with the RNA by either binding additional RNA sequence or increasing the number of contacts between the N-terminal residues and the canonical RRM to RNA. This hypothesis is supported by changes in the chemical shifts for residues in the RRM domain between Bruno RRM3+ and truncated RRM3. The largest changes in chemical shifts were observed for the residues of the central two β-strands, where the conserved RNP1 and RNP2 motifs are located. While the N-terminal residues do not form an ordered structure in the absence of RNA, their presence is sufficient to affect the local environment across the β-sheet of the RRM. If the chemical shift changes are due to transient interactions, then the N-terminal residues could be oriented in such a way to interact with the target RNA at the same time as the RRM domain interacts with target RNA.

In Bruno RRM3+, the combination of structural and RNA binding results, along with the flexibility of the N-terminal amino acids and chemical shift perturbations, suggests that these residues could function as an additional RNA binding surface, allowing the RNA to make additional contacts with the protein outside the canonical RRM. This expanded RNA binding surface could increase the sequence specificity or binding affinity. To more precisely identify the roles of the N-terminal extension, the costructure of the protein in complex with its target RNA is an ultimate goal. However, the specific sequence to which Bruno RRM3+ binds has not been clearly identified. The 140-nucleotide sequence used in binding would present a challenge due to the molecular weight limitations in NMR. Work is currently underway to further define the RNA sequence to which Bruno RRM3+ binds, which could facilitate further characterization of the structure and dynamics of this interaction. This is particularly important as the majority of characterized RRMs bind RNA in a sequence-specific manner, and each RRM must make a unique set of interactions with the target RNA. Previous work has demonstrated the importance of residues outside the central two β-strands in conferring RNA sequence specificity in RRMs (*7*, *44*, *47*, *53*, *54*). Thus, the N-terminal extension of Bruno RRM3+ may confer higher specificity to the binding

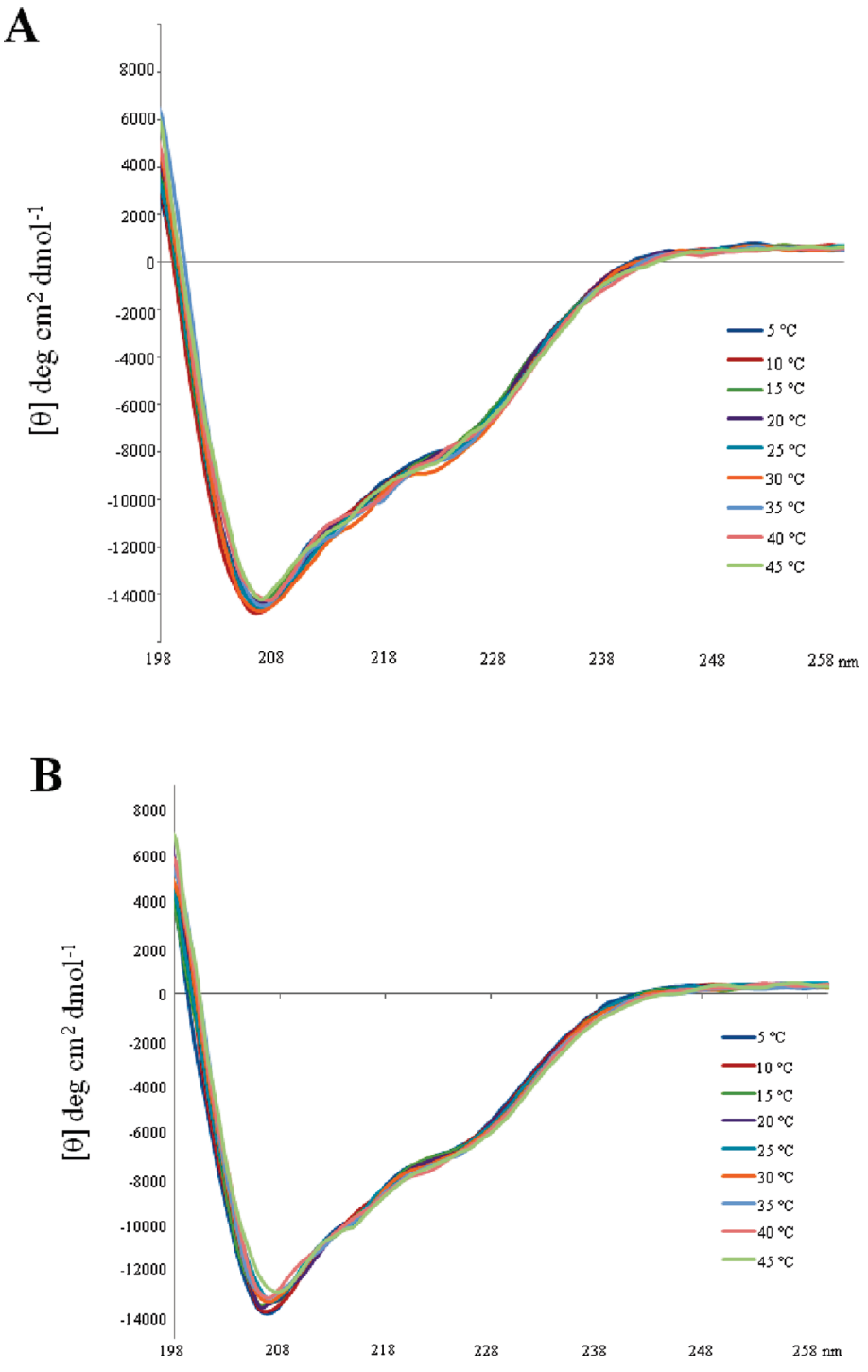

FIGURE 8: Circular dichroism spectra of Bruno RRM3+ and RRM3. The CD spectra of the two proteins are similar, and neither shows substantial temperature dependence in the range of 5−45 °C. Secondary structure predictions were obtained using SOMCD (*50*). The helix content of the two proteins is predicted to be in the 20 ± 10% range, which is consistent with the NMR-derived structures. (A) Overlaid CD spectra obtained for the Bruno RRM3+ protein. (B) CD spectra of the truncated Bruno RRM3 protein.

interaction, in addition to serving as an additional RNA binding site. Because RRMs are so prevalent, the RRM−RNA interactions that utilize only the canonical RRM may be insufficient to uniquely specify all of the required interactions (*1*−*3*, *6*, *7*).

Various RRM-containing proteins have been found to bind RNA with a wide range of affinities (*8*, *42*, *55*−*58*), and in many cases, the RNA binding partners of RRMs have not been identified. The studies of Bruno RRM3+ presented here raise the possibility that some of the weaker RNA-binding RRMs may require additional structural components to either allow or increase their affinity for RNA. These additional components could be provided by the same protein, as in the additional N-terminal residues of Bruno RRM3+, or perhaps by additional proteins via intermolecular interactions. Given the number of RRMs found in nature, and their involvement in diverse processes throughout cell maintenance, development, and differentiation, variations on the canonical RRM fold may be common. As in the case of Bruno RRM3+, other RRMs may also require additional RNA binding sites to increase the specificity and affinity of their interactions with RNA. Thus, an expanded view

of the canonical RRM motif may help to illuminate the mechanisms by which these proteins recognize RNA.

SUPPORTING INFORMATION AVAILABLE

Amide proton exchange rates for Bruno RRM3+ and RRM3, the sequence of the *oskar* AB RNA and a secondary structure diagram, representative NMR spectra, and ^{15}N NMR relaxation data. This material is available free of charge via the Internet at http://pubs.acs.org.

REFERENCES

1. Varani, G., and Nagai, K. (1998) RNA Recognition by RNP Proteins During RNA Processing. *Annu. Rev. Biophys. Biomol. Struct. 27*, 407–445.
2. Lunde, B. M., Moore, C., and Varani, G. (2007) RNA-binding proteins: Modular design for efficient function. *Nat. Rev. Mol. Cell Biol. 8*, 479–490.
3. Maris, C., Dominguez, D., and Allain, F. H.-T. (2005) The RNA recognition motif, a plastic RNA-binding platform to regulate post-transcriptional gene expression. *FEBS Lett. 272*, 2118–2131.
4. Nagai, K., Oubridge, C., Jessen, T. H., Li, J., and Evans, P. R. (1990) Crystal structure of the RNA-binding domain of the U1 small nuclear ribonucleoprotein A. *Nature 348*, 515–520.
5. Query, C. C., Bentley, R. C., and Keene, J. D. (1989) A Common RNA Recognition Motif Identified within a Defined U1 RNA Binding Domain of the 70K U1 snRNP Protein. *Cell 57*, 89–101.
6. Messias, A. C., and Sattler, M. (2004) Structural basis of single-stranded RNA recognition. *Acc. Chem. Res. 37*, 279–287.
7. Auweter, S. D., Oberstrass, F. C., and Allain, F. H.-T. (2006) Sequence-specific binding of single-stranded RNA: Is there a code for recognition? *Nucleic Acids Res. 34*, 4943–4959.
8. Burd, C. G., and Dreyfuss, G. (1994) Conserved Structures and Diversity of Functions of RNA Binding Proteins. *Science 265*, 615–621.
9. Siomi, H., and Dreyfuss, G. (1997) RNA-binding proteins as regulators of gene expression. *Curr. Opin. Genet. Dev. 7*, 345–353.
10. Kim-Ha, J., Kerr, K., and Macdonald, P. M. (1995) Translational Regulation of *oskar* mRNA by Bruno, an Ovarian RNA-Binding Protein, Is Essential. *Cell 81*, 403–412.
11. Webster, P. J., Liang, L., Berg, C. A., Lasko, P., and Macdonald, P. M. (1997) Translational repressor Bruno plays multiple roles in development and is widely conserved. *Genes Dev. 11*, 2510–2521.
12. Lipshitz, H. D., and Smibert, C. A. (2000) Mechanisms of RNA localization and translational regulation. *Curr. Opin. Genet. Dev. 10*, 476–488.
13. Snee, M., Benz, D., Jen, J., and Macdonald, P. M. (2008) Two distinct domains of Bruno bind specifically to the *oskar* mRNA. *RNA Biol. 5*, 1–9.
14. Barreau, C., Paillard, L., Mereau, A., and Osborne, H. B. (2006) Mammalian CELF/Bruno-like RNA-binding proteins: Molecular characteristics and biological functions. *Biochemie 88*, 515–525.
15. Good, P. J., Chen, Q., Warner, S. J., and Herring, D. C. (2000) A Family of Human RNA-binding Proteins Related to the *Drosophila* Bruno Translational Regulator. *J. Biol. Chem. 275*, 28583–28592.
16. Dev, A., Nayernia, K., Meins, M., Adham, I., Lacone, F., and Engel, W. (2007) Mice Deficient for RNA-Binding Protein Brunol1 Show Reduction of Spermatogenesis But Are Fertile. *Mol. Reprod. Dev. 74*, 1456–1464.
17. Delaunay, J., Le Mee, G., Ezzeddine, N., Labesse, G., Terzian, C., Capri, M., and Ait-Ahmed, O. (2004) The *Drosophila* Bruno paralog Bru-3 specifically binds the EDEN translational repression element. *Nucleic Acids Res. 32*, 3070–3082.
18. Yang, Y., Mahaffey, C. L., Berube, N., Maddatu, T. P., Cox, G. A., and Frankel, W. N. (2007) Complex Seizure Disorder Caused by *Brunol4* Deficiency in Mice. *PLoS Genet. 3*, 1275–1283.
19. Suzuki, H., Maegawa, S., Nishibu, T., Sugiyama, T., Yasuda, K., and Inoue, K. (2000) Vegetal localization of the maternal mRNA encoding and EDEN-BP/Bruno-like protein in zebrafish. *Mech. Dev. 93*, 205–209.
20. Hashimoto, Y., Suzuki, H., Kageyama, Y., Yasuda, K., and Inoue, K. (2006) Bruno-like protein is localized to zebrafish germ plasm during the early cleavage stages. *Gene Expression Patterns 6*, 201–205.
21. Suzuki, J., Jin, Y., Otani, H., Yasuda, K., and Inoue, K. (2002) Regulation of alternative splicing of α-actinin transcript by Bruno-like proteins. *Genes Cells 7*, 133–141.
22. Good, P. J. (1997) The role of *elav*-like genes, a conserved family encoding RNA-binding proteins, in growth and development. *Cell Dev. Biol. 8*, 577–584.
23. Wong, I., and Lohman, T. M. (1993) A double-filter method for nitrocellulose-filter binding: Application to protein-nucleic acid interactions. *Proc. Natl. Acad. Sci. U.S.A. 90*, 5428–5432.
24. Muhandiram, D. R., and Kay, L. E. (1994) Gradient-enhanced triple resonance three-dimensional NMR experiments with improved sensitivity. *J. Magn. Reson. Ser. B 103*, 203–216.
25. Grzesiek, S., and Bax, A. (1992) ^{1}H, ^{13}C, and ^{15}N NMR backbone assignments and secondary structure of human interferon-γ. *J. Magn. Reson. 96*, 432–440.
26. Kay, L. E. (1993) Pulsed-field gradient-enhanced three-dimensional NMR experiment for correlating $^{13}C^{\alpha}$, $^{13}C'$ and H^{α} chemical shifts in uniformly ^{13}C-labeled proteins dissolved in H_2O. *J. Am. Chem. Soc. 115*, 2055–2057.
27. Kay, L. E., Xu, G. Y., Singer, A. U., Muhandiram, D. R., and Forman-Kay, J. D. (1993) A gradient-enhanced HCCH-TOCSY experiment for recording side-chain ^{1}H and ^{13}C correlations in H_2O samples of proteins. *J. Magn. Reson. Ser. B 101*, 333–337.
28. Pascal, S. M., Muhandiram, D. R., Yamazaki, T., Forman-Kay, J. D., and Kay, L. E. (1994) Simultaneous acquisition of ^{15}N- and ^{13}C-edited NOE spectra of proteins dissolved in H_2O. *J. Magn. Reson, Ser. B 103*, 197–201.
29. Delaglio, F., Grzesiek, S., Vuister, G. W., Zhu, G., Pfeifer, J., and Bax, A. (1995) NMRPipe: A multidimensional spectral processing system based on UNIX pipes. *J. Biomol. NMR 6*, 277–293.
30. Wishart, D. S., Bigam, C. G., Yao, J., Abildgaard, F., Dyson, H. J., Oldfield, E., Markley, J. L., and Sykes, B. D. (1995) ^{1}H, ^{13}C, and ^{15}N chemical shift referencing in biomolecular NMR. *J. Biomol. NMR 6*, 135–140.
31. Farrow, N. A., Muhandiram, R., Singer, A. U., Pascal, S. M., Kay, C. M., Gish, G., Shoelson, S. E., Pawson, T., Forman-Kay, J. D., and Kay, L. E. (1994) Backbone dynamics of a free and phosphopeptide-complexed Src homology 2 domain studied by ^{15}N NMR relaxation. *Biochemistry 33*, 5984–6003.
32. Lipari, G., and Szabo, A. (1982) Model-free approach to the interpretation of nuclear magnetic resonance relaxation in macromolecules. 1. Theory and range of validity. *J. Am. Chem. Soc. 104*, 4546–4559.
33. Palmer, A. G.III, Rance, M., and Wright, P. E. (1991) Intramolecular motions of a zinc finger DNA binding domain from Xfin characterized by proton-detected natural abundance carbon-13 heteronuclear NMR spectroscopy. *J. Am. Chem. Soc. 113*, 4371–4380.
34. Mandel, A. M., Akke, M., and Palmer, A. G.III (1995) Backbone dynamics of *Escherichia coli* ribonculease HI: Correlations with structure and function in an active enzyme. *J. Mol. Biol. 246*, 144–163.
35. Lillemoen, J., and Hoffman, D. W. (1998) An investigation of the dynamics of ribosomal protein L9 using heteronuclear NMR relaxation measurements. *J. Mol. Biol. 291*, 539–551.
36. Lillemoen, J., Cameron, C. S., and Hoffman, D. W. (1997) The Stability and Dynamics of Ribosomal Protein L9: Investigations of a Molecular Strut by Amide Proton Exchange and Circular Dichroism. *J. Mol. Biol. 268*, 482–493.
37. Bai, Y., Milne, J. S., Mayne, L., and Englander, S. W. (1993) Primary Structure Effects on Peptide Group Hydrogen Exchange. *Proteins: Struct. Funct. Genet. 17*, 75–86.
38. Roder, H., Wagner, G., and Wutrich, K. (1985) Amide proton-exchange in proteins by EX1 kinetics: Studies of the basic pancreatic trypsin inhibitor at variable p^2H and temperature. *Biochemistry 24*, 7396–7407.
39. Bai, Y., Englander, J., Mayne, L., Milne, J. S., and Englander, S. W. (1995) Thermodynamic parameters from hydrogen exchange measurements. In Methods in Enzymology (Johnson, M. L., and Acker, G. K., Eds.) Vol. 259, pp 344−356, Academic Press, New York.
40. Molday, R. S., Englander, S. W., and Kallen, R. G. (1972) Primary structure effects of peptide group hydrogen exchange. *Biochemistry 11*, 150–158.
41. Brünger, A. T.; et al. (1998) Crystallography and NMR System: A new software suite for macromolecular structure determination. *Acta Crystallogr. D54*, 905–921.
42. Berjanskii, M. V., Neal, S., and Wishart, D. S. (2006) PREDITOR: A web server for predicting torsion angle restraints. *Nucleic Acids Res. 34*, W63–W69.
43. Oubridge, C., Ito, N., Teo, C. H., and Nagai, K. (1994) Crystal structure at 1.92 Å of the RNA-binding domain of the U1A spliceosomal protein complexed with an RNA hairpin. *Nature 372*, 432–438.
44. Avis, J. M., Allain, F. H., Howe, P. W., Varani, G., Nagai, K., and Neuhaus, D. (1996) Solution Structure of the N-terminal RNP

Domain of U1A Protein: The Role of C-terminal Residues in Structure Stability and RNA Binding. *J. Mol. Biol. 257*, 398–411.
45. Howe, P. W. A., Nagai, K., Neuhaus, D., and Varani, G. (1994) NMR Studies of U1 snRNA recognition by the N-terminal RNP domain of the human U1A protein. *EMBO J. 13*, 3873–3881.
46. Showalter, S., and Hall, K. B. (2002) A Functional Role for Correlated Motion in the N- terminal RNA-binding Domain of Human U1A Protein. *J. Mol. Biol. 322*, 535–542.
47. Kranz, J. K., and Hall, K. B. (1999) RNA Recognition by the Human U1A Protein is Mediated by a Network of Local Cooperative Interactions That Create the Optimal Binding Surface. *J. Mol. Biol. 285*, 215–231.
48. Handa, N., Nureki, O., Kurimoto, K., Kim, I., Sakamoto, H., Shimura, Y., Moto, Y., and Yokoyama, S. (1999) Structural basis for recognition of the tra mRNA precursor by the Sex-lethal protein. *Nature 398*, 579–585.
49. Tsuda, K., Kuwasako, K., Takahashi, M., Someya, T., Terada, T., Kobayashi, N., Shirouzu, M., Kigawa, T., Tanaka, A., Sugano, S., Guntert, P., Muto, Y., and Yokoyama, S. (2009) Structural basis for the sequence-specific RNA-recognition mechanism of human CUG-BP1 RRM3. *Nucleic Acids Res. 37*, 5151–5166.
50. Unneberg, P., Merelo, J. J., Chacon, P., and Moran, F. (2001) SOMCD: Method for evaluating protein secondary structure from UV circular dichroism spectra. *Proteins: Struct. Funct. Genet. 42* (4), 460–470.
51. Conte, M. R., Grune, T., Ghuman, J., Kelly, G., Ladas, A., Matthews, S., and Curry, S. (2000) Structure of tandem RNA recognition motifs from polypyrimidine tract binding protein reveals novel features of the RRM fold. *EMBO J. 19*, 3132–3141.
52. Oberstrass, F. C., Auweter, S. D., Erat, M., Hargous, Y., Henning, A. Wenter, P., Reymond, L., Amir-Ahmady, B., Pitsch, S., Black, D. L., and Allain, F. H.-T. (2005) Structure of PTB Bound to RNA: Specific Binding and Implications for Splicing Regulation. *Science 309*, 2054–2057.
53. Zeng, Q., and Hall, K. B. (1997) Contribution of the C-terminal tail of U1A RBD1 to RNA recognition and protein stability. *RNA 3*, 303–314.
54. Kranz, J. K., and Hall, K. B. (1998) RNA Binding Mediates the Local Cooperatively between the B-Sheet and the C-Terminal Tail of the Human U1A RBD1 Protein. *J. Mol. Biol. 275*, 465–481.
55. Deo, R. C., Bonnano, J. B., Sonenberg, N., and Burley, S. K. (1999) Recognition of polyadenylate RNA by the poly(A)-binding protein. *Cell 98*, 835–845.
56. Nietfeld, W., Mentzel, H., and Pieler, T. (1990) The *Xenopus laevis* poly(A) binding protein is composed of multiple functionally independent RNA binding domains. *EMBO J. 9*, 3699–3705.
57. Burd, C. G., Matinus, E. L., and Dreyfuss, G. (1991) The Multiple RNA-Binding Domains of the mRNA Poly(A)-Binding Protein Have Different RNA-Binding Activities. *Mol. Cell. Biol. 11*, 3419–3424.
58. Kuhn, U., and Peiler, T. (1996) *Xenopus* Poly(A) Binding Protein: Functional Domains in RNA Binding and Protein-Protein Interaction. *J. Mol. Biol. 256*, 20–30.
59. DeLano, W. L. (2002) The PyMol Molecular Graphics System, DeLano Scientific, San Carlos, CA.
60. Zuker, M. (2003) Mfold web server for nucleic acid folding and hybridization prediction. *Nucleic Acids Res. 31*, 3406–1415.
61. Mathews, D. H., Sabina, J., Zuker, M., and Turner, D. H. (1999) Expanded Sequence Dependent of Thermodynamic Parameters Improves Prediction of RNA Secondary Structure. *J. Mol. Biol. 288*, 911–940.